Journal of Luminescence 294 (2026) 121831

Contents lists available at ScienceDirect

Journal of Luminescence

journal homepage: www.elsevier.com/locate/jlumin

Luminescent thermometry using borogermanate glass doped with europium recovered from electronic waste

Fábio J. Caixeta [a], Ana Elisa Berno [a], Marina P. Abuçafy [a], Elias P. Ferreira-Neto [a], Leonardo V. Albino [a,b], Thiago A. Lodi [a], Marcelo Nalin [a], Estevam C. Marques [a], Aline M. Feltran [a], Ana Beatriz Acosta [c], Vitor dos S.de Souza [c], Rogéria R. Gonçalves [c], Sidney J.L. Ribeiro [a,*], Douglas F. Franco [a,**]

[a] São Paulo State University (UNESP), Institute of Chemistry, Araraquara, Brazil
[b] São Carlos Institute of Chemistry (IQSC), University of São Paulo (USP), São Carlos, SP, 13566-590, Brazil
[c] Centro de Nanotecnologia e Engenharia Tecidual - Laboratório Mater Lumen, Departamento de Química, FFCLRP, Universidade de São Paulo, Ribeirão Preto, SP, Brazil

ARTICLE INFO

Keywords:
Temperature sensing
Primary thermometer
LIR
Eu(III) luminescence
Rare earth
Urban mining

ABSTRACT

Borogermanate glasses doped with Eu^{3+} ions are promising materials for luminescent thermometry due to their high thermal stability and optical properties. Recovering rare-earth elements from electronic waste (e-waste) offers a sustainable source for such functional materials. Here we synthesized a borogermanate glass incorporating 30 wt% e-waste-derived Eu^{3+} ions via melt-quenching and characterized its photoluminescence behavior for temperature sensing. The glass exhibited characteristic Eu^{3+} emission transitions with temperature-dependent luminescence intensity ratio (LIR) between thermally coupled $^7F_0$ and $^7F_2$ energy levels, following Boltzmann distribution in the 300-400 K range. The energy gap was determined as 926 ± 44 cm^{-1}, with a maximum relative thermal sensitivity of 1.48 % K^{-1} at 300 K and a temperature uncertainty of 1.7 K. The obtained primary luminescence thermometer proved to be stable under cyclic temperature changes. At 400 K, a mean LIR value of 0.16545 was obtained, with a standard deviation of 0.00277 (RSD = 1.67%). These findings demonstrate that borogermanate glasses derived from e-waste can serve as sustainable and reliable primary luminescent thermometers for advanced optical sensing applications.

1. Introduction

The increasing global demand for rare-earth elements (REE) [1,2] - essential components in advanced photonic, electronic, and energy-conversion technologies [3–7] - has intensified both environmental and geopolitical concerns. More than 80% of REE production and processing currently occur in a few countries, particularly China, which dominates the global supply chain [8–10]. This concentration leads to significant vulnerabilities, such as supply risks, price volatility, and trade restrictions, directly impacting industries and research sectors worldwide. Moreover, conventional mining and refining of REE generate substantial environmental damage, including toxic waste, soil degradation, and water contamination [11].

In response to these challenges, obtaining high value-added technological elements such as REE from electronic waste (the so-called "urban mining") emerges as an environmentally viable alternative, enabling the recovery of discarded permanent magnets and fluorescent lamps, promoting circular economy principles, and reducing dependence on primary natural sources. Beyond sustainability, urban mining offers an opportunity to produce functional materials with high technological performance while mitigating geopolitical and ecological risks [12,13].

The possibility of manipulating the glass composition based on heavy metal oxide (HMO) glasses by RE ions can induce structural changes in the glass network and, generally, contribute directly to electrical, optical, and magneto-optical (MO) properties [14–16]. Borogermanate glasses have been highlighted in recent years for their high thermal stability and ability to solubilize high concentrations of RE ions, thereby

This article is part of a special issue entitled: The 60th anniversary of Prof. Luís D. Carlos published in Journal of Luminescence.

* Corresponding author.
** Corresponding author.
E-mail addresses: sidney.jl.ribeiro@unesp.br (S.J.L. Ribeiro), douglas.franco@unesp.br (D.F. Franco).

https://doi.org/10.1016/j.jlumin.2026.121831
Received 27 November 2025; Received in revised form 11 February 2026; Accepted 26 February 2026
Available online 12 March 2026

preventing crystal or cluster formation. Our research group recently reported the synthesis and characterization of MO borogermanate glasses doped with varying concentrations of a complex matrix based on fluorescent lamps waste, which contains several chemical elements, among them Eu^{3+} and Tb^{3+} ions [12]. The glasses synthesized do not present crystal or cluster formation and exhibit characteristic Eu^{3+} and Tb^{3+} optical and magnetic properties. Their maximum Verdet constant (V_B) value at 632.8 nm was −40.9 rad T^{-1} m^{-1} [12]. To the best of our knowledge, this was the first-time report on magnetic-optical glasses prepared from electronic waste. The development of such photonic materials derived from recovered REE thus bridges sustainability with technological innovation, opening new possibilities for advanced optical applications such as luminescent thermometry.

Temperature measurement is fundamental across scientific, industrial, and biomedical processes, as it directly governs the kinetics, thermodynamic stability, and overall behaviour of physical, chemical, and biological systems [17,18]. Conventional temperature sensors often require direct contact with the sample, which can be impractical or even impossible under specific conditions such as harsh environments, miniaturized systems, or biological tissues [19]. These limitations have driven significant interest toward non-contact temperature sensing strategies, including infrared thermography and luminescent thermometry. While infrared thermography is widely used, its performance strongly depends on the emissivity of the material and is limited by poor spatial resolution [20,21]. In contrast, luminescent thermometry offers unique advantages, such as high spatial and temporal resolution, resistance to electromagnetic interference, and compatibility with micro- and nanoscale environments [22].

Luminescent thermometers rely on the temperature dependence of optical parameters such as emission intensity, lifetime, band shift, or the ratio between two thermally coupled transitions, commonly known as the luminescence intensity ratio (LIR) [23]. Among the various luminescent probes, trivalent RE ions (RE^{3+}) are particularly attractive due to their sharp emission lines, long-lived excited states, and multiple thermally coupled energy levels spanning the UV to near-infrared range [24]. The choice of the RE^{3+} ion and host matrix determine the operational temperature range, sensitivity, and stability of the thermometer [4,22,25–27].

Europium ion (Eu^{3+}) stands out as an efficient optical center for luminescent thermometry because of its well-defined emission bands arising from the $^5D_0 \rightarrow {}^7F_J$ (J = 0-6) transitions in the visible region. The relative populations of the Stark sublevels within the ^7F_J manifold can vary with temperature, enabling the use of LIR-based strategies to estimate temperature changes [28]. Recent studies have demonstrated that Eu^{3+}-based materials can achieve competitive sensitivities within the physiological temperature range, making them promising candidates for applications in biomedicine and photonic devices [29].

The performance of Eu^{3+} thermometers strongly depend on the host matrix, which should ensure low phonon energy to minimize non-radiative losses and provide chemical and thermal stability [30]. In this context, borogermanate (BGeB) glasses have attracted attention due to their high refractive index, excellent transparency in the visible region, good thermal stability, and high rare-earth solubility [12,31–33]. Furthermore, their glass-forming ability and structural flexibility allow homogeneous incorporation of rare-earth ions without clustering effects, preserving the luminescent properties of Eu^{3+} [34].

In this work, we report a detailed study on the luminescent thermometric behavior of Eu^{3+}-doped borogermanate glass (BGeB:Eu^{3+}). The thermometric analysis was carried out using the LIR approach, based on the temperature-dependent redistribution of populations among the ^7F_J levels and their influence on the $^5D_0 \rightarrow {}^7F_J$ transition intensity. The measurements were performed over a temperature range relevant for photonic and optoelectronic applications. These results provide new insights into the potential of BGeB:Eu^{3+} glasses as luminescent thermometers for advanced sensing technologies. This may be the first promising vitreous luminescent thermometer made from recovered fluorescent lamp waste.

2. Experimental section

2.1. Glass preparation

The bulk BGeB glass was synthesized according to the conventional melt-quenching method from the chemical precursors germanium oxide (99.9%, Sigma-Aldrich), boron oxide (99.9%, Sigma-Aldrich), barium carbonate (99.9%, Sigma-Aldrich), aluminum oxide (99.9%, Sigma-Aldrich) and sodium carbonate (99.9%, Sigma-Aldrich). All precursors were stoichiometrically weighed out to give 10 g based on $41GeO_2$-$25B_2O_3$-$4Al_2O_3$-$10Na_2O$-20BaO)-30%wst (or BGeB-30%wst), where 30% represents the proportion of fluorescent lamp waste (in wt%) incorporated into the BGeB glass matrix [12]. The glass composition was homogenized in a FlackTek speed mixer machine and loaded into a platinum crucible. It was then thermally treated at 850 °C for 30 min to ensure the complete thermal decomposition of barium and sodium carbonates into their corresponding oxides. Subsequently, the composition was melted at 1400 °C for 90 min in a resistive furnace under atmospheric conditions. After melting, the mixture was cooled in preheated stainless-steel molds at 30 °C below the glass transition temperature for 6 h to minimize mechanical stress. As a result, a BGeB-30% wst glass with a thickness of approximately 2 mm was obtained. As a final step, the glass sample was polished using silicon carbide (SiC) paper with grit sizes of 600, 800, and 2400 mesh prior to optical characterization.

2.2. Characterizations

Differential Scanning Calorimetry (DSC) measurements were carried out from 400 to 900 °C in a Netzsch DSC 404 F3 Pegasus calorimeter under a 20 mL min^{-1} nitrogen atmosphere, at a heating rate of 10 °C min^{-1} and using platinum crucibles. The maximum errors for the glass transition temperature (T_g) are ± 2 °C.

Powder X-ray Diffraction (XRD) analyses were performed at room temperature in a Bruker D8 Advance model diffractometer equipped with a Ni filter, with Cu Kα radiation (1.54186 Å). The measurements were recorded in the 2θ range from 5 to 90°, with a 0.020° scan step and using a scanning speed of 5° min^{-1}.

Photoluminescence (PL) excitation and emission spectra were recorded at room temperature and under heating on a Horiba-Jobin Yvon Fluorolog®-3 FL3-22 spectrofluorometer equipped with a Hamamatsu R928P photomultiplier as UV-visible detector. The excitation source was a 450 W continuous xenon short-arc lamp (UXL-450S-O, USHIO INC.). The PL emission spectra have been corrected for the wavelength sensitivity of the detector and the PL excitation spectra to the intensity of the xenon lamp in the excitation range. The conversion from wavelength to energy units (cm^{-1}) using the Jacobian transformation of the intensity values were performed [35].

Temperature-dependent PL measurements were carried out using a homemade cryostat-oven accessory (1.0 K accuracy) coupled to a FLYEVER Equipments temperature controller (model FE50RPN). The cryostat-oven was designed by Microtube company. The temperature of the sample was increased at a heating rate of 1 K min^{-1} by means of an electrical resistance and it was lowered by the addition of liquid N_2. The thermalization time was 3 min.

3. Results and discussion

Thermal, structural, optical, and magneto-optical characterizations of BGeB-%wst glass system containing fluorescent lamp waste (wst) were previously investigated in previous study of our group by Berno et al. [12]. The glasses were synthesized with the composition ($41GeO_2$–$25B_2O_3$–$4Al_2O_3$–$10Na_2O$–20BaO)–x%wst, where x = 0, 10, 20, 30, and 50.

In this case, from the analysis of the DSC curve for the BGeB-30%wst glass, it was possible to extract the main characteristic temperature, the glass transition (T_g), equal to 649 °C (Figure SI1). XRD pattern for the BGeB-30%wst sample showed the presence of a diffuse halo and the absence of narrow peaks, indicating a non-crystalline nature (Figure SI2). The presence of a T_g and a non-crystalline behavior confirms the vitreous nature of the sample analyzed.

In our previous study, increasing e-waste content caused a slight decrease in optical transmittance, whereas all samples exhibited intense visible photoluminescence associated with characteristic Tb^{3+} and Eu^{3+} transitions [12]. Based on these results, the BGeB-30%wst glass was selected for the present luminescent thermometry investigation due to its high visible transmittance and relatively elevated Eu^{3+} content (0.27 wt%). These characteristics make it a promising candidate for temperature-sensing applications based on Eu^{3+} photoluminescence.

Fig. 1a presents PL excitation spectrum of BGeB-30%wst glass sample at room temperature (RT, 298 K) and monitoring the emission at 704.0 nm (Eu^{3+}:$^5D_0 \rightarrow {}^7F_4$). The spectrum consists of a broad band in the 250-350 nm region, corresponding to energy transfer from the host matrix to Eu^{3+} energy levels, and Eu^{3+} intraconfigurational 4f-4f transitions. Excitation bands were mainly observed at 393.0, 464.0, 524.0, and 531.0 nm, which are assigned to Eu^{3+} transitions coming from $^7F_0$ ground state and $^7F_1$ energy level to $^5L_6$, $^5D_2$, and $^5D_1$ excited states, respectively. The energy of 380 cm^{-1} for Eu^{3+}:$^7F_1$ energy level [36] allows its population even at room temperature. As it can be verified at 531.0 nm in Fig. 1a, $^7F_1 \rightarrow {}^5D_1$ transition. On the other hand, any expressive excitation bands ascribed to transitions coming from Eu^{3+}:$^7F_2$ excited energy level, 1043 cm^{-1} [36] are verified in the excitation spectrum of Fig. 1a. Fig. 1b displays a partial energy levels diagram of Eu^{3+} [37] along with the excitation and emission mechanisms verified in Fig. 1a and throughout this work. Double arrows indicate both excitation and emission transitions.

For a luminescence thermometer containing only one luminescent center, the temperature can be determined from the ratio of the excitation/emission intensities of two electronic transitions. The electronic populations of these two thermally coupled energy levels can be obtained from the Boltzmann thermal equilibrium model [25,38]. Fig. 2a depicts a schematic energy level diagram with the thermally coupled energy levels of Eu^{3+}. The broad arrow in Fig. 2a, didactically, illustrates the direction of the electronic population (N) variation in the thermally coupled levels with increasing temperature. An increase in temperature lead to depopulation of $|0\rangle$ energy level. Contrarily, it is expected that N

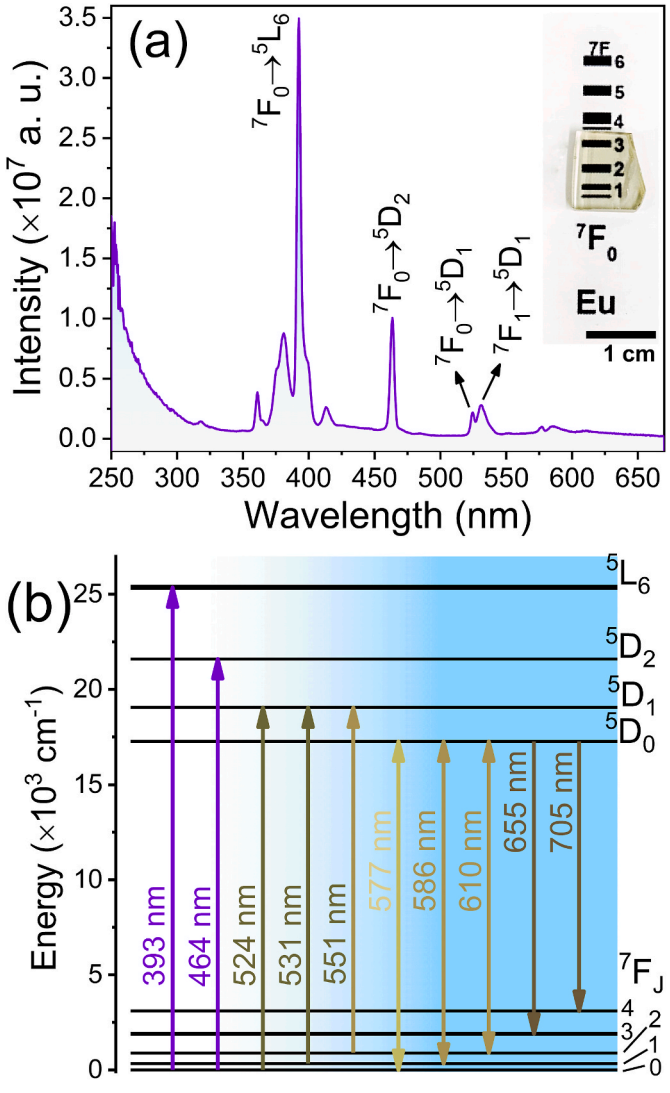

Fig. 1. (a) PL excitation spectra of BGeB-30%wst sample at room temperature and monitoring the emission at 704.0 nm. Inset: Photograph of the BGeB-30% wst glass sample under exposure to ambient lighting. (b) Partial energy levels diagram of Eu^{3+} ion.

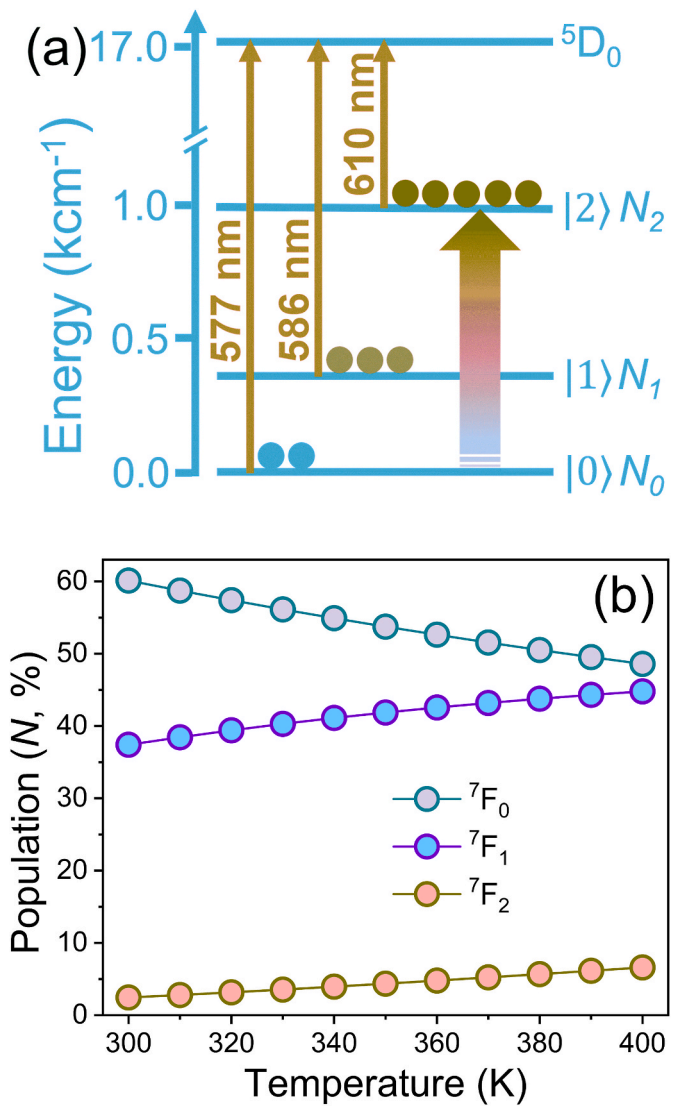

Fig. 2. (a) Schematic diagram of the thermally coupled energy levels of Eu^{3+} ion and the respective N as a function of the temperature and (b) Fractional population of ^7F_J energy levels as a function of absolute temperature.

rises in the |1⟩ and |2⟩ energy levels. For Eu^{3+} ion, |0⟩, |1⟩, and |2⟩ correspond to $^7F_0$, $^7F_1$, and $^7F_2$ energy levels, respectively [19]. Fig. 2a shows electronic transitions coming from the thermally coupled levels to $^5D_0$ excited energy level. For BGeB-30%wst glass the $^7F_0 \rightarrow {}^5D_0$, $^7F_1 \rightarrow {}^5D_0$, and $^7F_2 \rightarrow {}^5D_0$ intraconfigurational *f-f* transitions are observed, respectively, at 577, 586, and 610 nm in Fig. 1a.

The electron population of ^7F_J energy levels is predicted by Boltzmann distribution [38]. In this sense, the electronic population of two thermally coupled levels is given by Equation (1) [38,39].

$$N_2 = N_1\left(\frac{g_2}{g_1}\right)exp\left(\frac{-\Delta E}{k_B T}\right) \quad (1)$$

Where N_2 and N_1 are the electronic population of thermally coupled energy levels |2⟩ and |1⟩, g_2 and g_1 are the barycenters of these levels, ΔE is the energy difference, and k_B is the Boltzmann constant.

The level energies (in cm^{-1}) of $^7F_0$, $^7F_1$, and $^7F_2$ were obtained using excitation spectrum presented hereafter and they are 0, 328, and 1002 cm^{-1}, respectively. Fig. 2b displays the calculated fractional population (in %) of $^7F_0$, $^7F_1$, and $^7F_2$ Eu^{3+} energy levels in the 300-400 K range using the general form of Boltzmann distribution for the fractional population of particles [25,39–41]. Therefore, as $^7F_0$, $^7F_1$, and $^7F_2$ are thermally populated Eu^{3+} levels, BGeB-30%wst glass sample was submitted to heating and PL excitation spectra were collected.

Fig. 3a and b shows the obtained excitation spectra of BGeB-30%wst glass sample at 300, 353, and 403 K in the 450.0-625.0 nm (a) and 573.0-622.0 nm (b) spectral range. It is possible to observe bands related to transitions coming from $^7F_0$ and $^7F_1$ decreasing in intensity with temperature increase. On the other hand, bands located at 551.0 and 610.0 nm, which are assigned to transitions from $^7F_2$, emerged for 353 K and 403 K.

To corroborate the results presented in the excitation spectra of Fig. 3a and b, emission spectra were obtained at 300 and 400 K. Fig. 3c and d presents the temperature influence in the PL emission of BGeB-30%wst glass and under excitation at 392.5 nm ($^7F_0 \rightarrow {}^5L_6$) and 610.0 nm ($^7F_2 \rightarrow {}^5D_0$), respectively. Under excitation at 392.5 nm (Fig. 3c), the emission of BGeB-30%wst sample decreased approximately 38% when the temperature increased from 300 K to 400 K. In opposition to this, the emission increased approximately 81% for excitation at 610.0 nm and at the same 300 K to 400 K temperature variation of BGeB-30%wst glass (Fig. 3d).

To better realize the temperature-dependent PL, emission spectra of BGeB-30%wst glass were acquired each 10 K increment in the 300-400 K range. Fig. 4a and b displays the obtained spectra for excitation at $^7F_0 \rightarrow {}^5L_6$ transition (392.5 nm) and at $^7F_2 \rightarrow {}^5D_0$ transition (610.0 nm). As expected, the PL intensity decreased under excitation at 392.5 nm ($^7F_0 \rightarrow$), and it increased for excitation at 610.0 nm ($^7F_2 \rightarrow$). For better display the variation of PL emission according to the temperature, the spectra of Fig. 4a and b were integrated, and it is graphically displayed in Fig. 4c. Figure SI3 shows the emission spectra of Fig. 4a and b after conversation to energy units (cm^{-1}) and Jacobian Transformation to the intensity [35].

As the PL emission intensity is proportional to the population of the thermally coupled energy levels, Equation (1) can be realized as a ratiometric thermal parameter. Thus, the Luminescence Intensity Ratio (*LIR*) is given by Equation (2) [42].

$$LIR = \frac{I_{\lambda exc=610nm}}{I_{\lambda exc=393nm}} = B\,exp\left(\frac{-\Delta E}{k_B T}\right) \quad (2)$$

Fig. 4d presents *LIR* values as a function of the temperature of BGeB-30%wst sample. A linear behavior is observed, with an adjusted R-Square (r^2) higher than 0.9961. The error of *LIR* (δ_{LIR}) was calculated using Equation (3) [38]. Herein, the main contribution to uncertainty of integrated emission area is related signal-to-noise ratio. Therefore, the error of *LIR* was obtained by the difference of the non-smoothed and smoothed spectra of Fig. 4. The temperature-dependent PL emission spectra were smoothed on OriginPro® software using Savitzky-Golay smoothing method [43], with a 2nd-order polynomial and points of window equal to 10. Figure SI4 (Supplementary information) presents the smoothed spectra for excitation at 610.0 nm.

$$\delta_{LIR} = LIR \times \sqrt{\left(\frac{\delta A_{610}}{A_{610}}\right)^2 + \left(\frac{\delta A_{393}}{A_{393}}\right)^2} \quad (3)$$

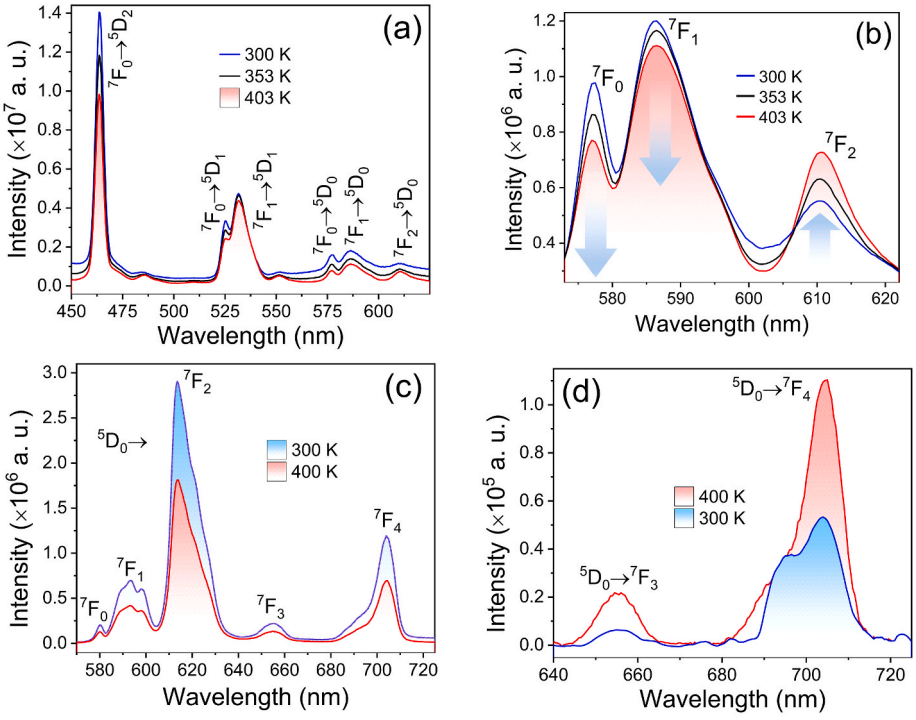

Fig. 3. Temperature-dependent PL of BGeB-30%wst glass for (a-b) excitation spectra monitoring the emission at 704.0 nm and (c-d) emission spectra for excitation at 392.5 and 610.0 nm.

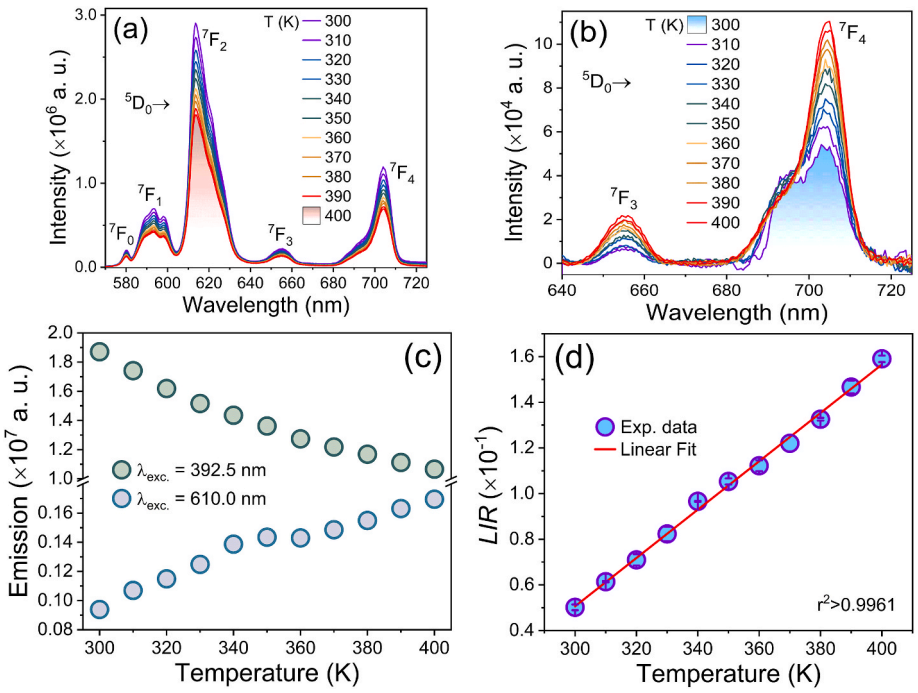

Fig. 4. PL emission spectra of BGeB-30%wst glass as a function of temperature for excitation at (a) 392.5 nm and (b) 610.0 nm. (c) Integrated emission of $^7D_0\rightarrow{}^7F_3$ and $^5D_0\rightarrow{}^7F_4$ transitions and (d) Dependence of *LIR* on the experimental temperature. The solid line represents the best linear fit to the experimental data.

Fluorescent lamp waste-derived rare earth sources may introduce additional lanthanide ions, such as Tb^{3+}, which can affect the luminescent properties of Eu^{3+}. As reported in our previous work [12], both Tb^{3+} and Eu^{3+} emissions were observed, together with non-radiative energy transfer (ET) processes between the host matrix and these Ln^{3+} ions, as well as interionic ET ($Tb^{3+}\rightarrow Eu^{3+}$). These interactions arise from overlap between the Tb^{3+} $^5D_4$ energy level and the Eu^{3+} excited states and can modify excitation pathways and emission intensities. In the present study, however, the thermometric performance relies on the luminescence intensity ratio (LIR) between Eu^{3+} emissions originating from thermally coupled energy levels, which is governed by the Boltzmann population distribution. Since the monitored mechanism in this work is intrinsic to the Eu^{3+} energy-level structure, the presence of other rare earth ions does not alter the energy gap between the coupled Eu^{3+} levels, nor the fundamental temperature dependence of the LIR.

The energy difference (*ΔE*) between the thermally coupled $^7F_0$ and $^7F_2$ energy levels of Eu^{3+} ion can be graphically obtained by applying natural logarithm (Ln) to both sides of Equation (2). Therefore, the slope of the graph is equal to $\Delta E/ k_B$, Equation (4).

$$ln\ LIR = ln\ B - \frac{\Delta E}{k_B}\times\frac{1}{T} \tag{4}$$

Fig. 5a shows ln *LIR vs.* 1/T for the BGeB-30%wst glass in the 300-400 K range. The slope of the graph presented in Fig. 5a is equal to 1332, that is, $\Delta E/ k_B = 1332$. Here the Boltzmann constant is 0,69503476 cm^{-1} K^{-1}. Therefore, $\Delta E = 1332*0{,}6950376 = 926 \pm 44$ cm^{-1}. ΔE can also be calculated by the difference among the barycenters of $^7F_0\rightarrow{}^5D_0$ and $^7F_2\rightarrow{}^5D_0$ transitions. Fig. 5b depicts Gaussian fit of $^7F_0\rightarrow{}^5D_0$ and $^7F_2\rightarrow{}^5D_0$ transition in the excitation spectra obtained at 403 K and monitoring the emission at 704.0 nm. The barycenter energy of $^7F_0\rightarrow{}^5D_0$ is 17352 cm^{-1}, while it is 16350 cm^{-1} for $^7F_2\rightarrow{}^5D_0$ transition. Thereby, an energy difference of 1002 cm^{-1} is calculated, which is good agreement with the value determined graphically (926 ± 44 cm^{-1}, Fig. 5a). In the literature, it has been observed ΔE of 969 cm^{-1} and 1036 cm^{-1} for Eu^{3+}-doped alumino-phosphate glass [42], whereas 1043 cm^{-1} was calculated for the free ion levels [36,44].

At room temperature (RT/T_0), Equation (2) can be expressed as:

$$LIR_0 = \frac{I_{\lambda exc=610nm}}{I_{\lambda exc=393nm}} = B\ exp\left(\frac{-\Delta E}{k_B T_0}\right) \tag{5}$$

Taking the ratio of Equation (2) and Equation (5), applying the natural logarithm, and rearranging the expression, it is possible to obtain an equation for the calculation of temperature from the PL measurements, Equation (6). Thus, luminescence thermometers that make use of a well-established equation of state and that allow the absolute temperature to be obtained directly from an experimental parameter (LIR) and without the need for calibration are the so-called primary thermometers [38].

$$\frac{1}{T} = \frac{1}{T_0} - \frac{k_B}{\Delta E} ln\left(\frac{LIR}{LIR_0}\right) \tag{6}$$

Fig. 6a presents calculated temperatures using Equation (6) for the experimental *LIR* values of BGeB-30%wst glass ranging from 0.050 to 0.159. Fig. 6a also displays the temperature reading using a thermocouple (experimental temperature). A good agreement among calculated and experimental temperatures was obtained, indicating that an efficient luminescence primary thermometer was obtained.

The performance of a luminescence thermometer can be evaluated by parameters as relative thermal sensitivity (Sr) and temperature uncertainty (δT) [17,38]. Thermal sensitivity indicates the variation, in percentage, of the thermometric parameter (LIR) when the temperature increases by 1 K, Equation (9). Thus, its unit is % K^{-1} or %/K. Fig. 6b presents the obtained relative thermal sensitivity values calculated using Equation (9), in the 300-400 K range. The maximum *Sr* value was 1.48% K^{-1}, at 300 K. In the literature, luminescence thermometer based on Eu^{3+}-doped alumino-phosphate glass has provided *Sr* values between 1.68 and 1.25 % K^{-1} at 288 K and 333 K, respectively [28,42].

As far as we know, there are no reported luminescence thermometers based on Eu^{3+}-doped materials where this ion was recovered from waste. Nevertheless, Table 1 presents examples of relative thermal sensitivity for different luminescence thermometers based on Eu^{3+} thermally coupled energy levels. Most of the reposted *Sr* values are those based on $^5D_1$ and $^5D_0$ energy levels, yielding *Sr* values from 0.5 to 2.75 % K^{-1}. Ordinarily, luminescence thermometers that employ $^5D_1$ and $^5D_0$

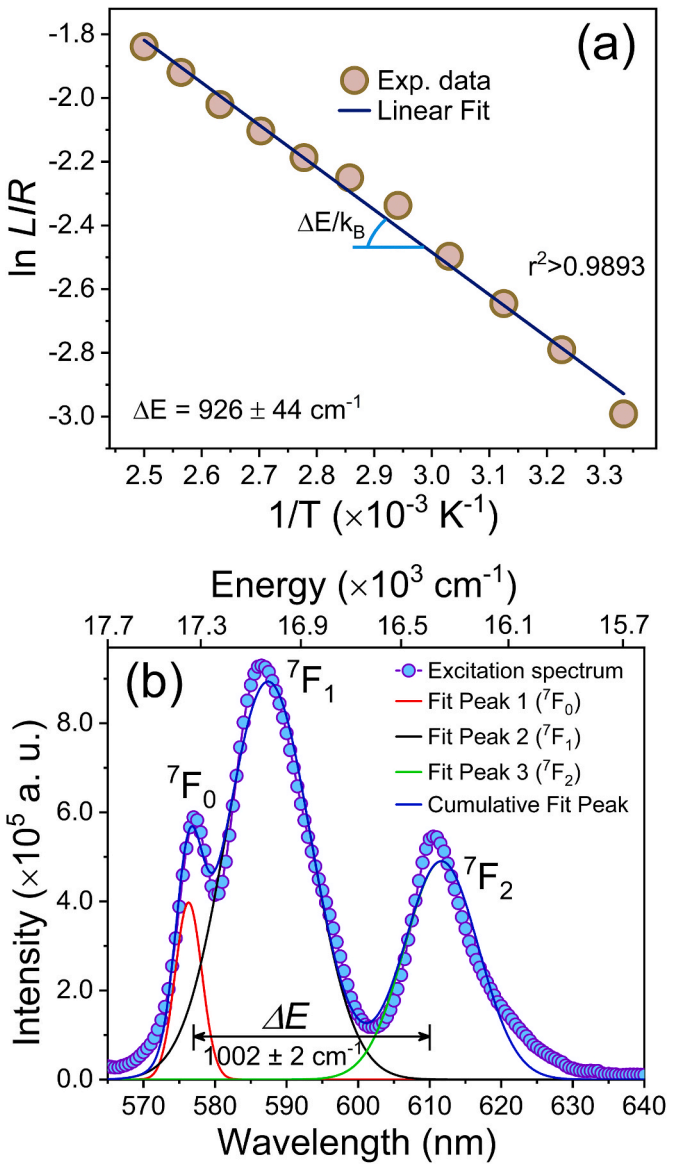

Fig. 5. (a) Dependence of ln *LIR* on the experimental temperature. The solid line represents the best linear fit to the experimental data. (b) Gaussian fit of $^7F_0 \rightarrow {}^5D_0$ and $^7F_2 \rightarrow {}^5D_0$ transitions in the PL excitation spectra.

($\Delta E \approx 1700\ cm^{-1}$) exhibit higher relative thermal sensitivity then those based on $^7F_2$ and $^7F_0$ ($\Delta E \approx 1000\ cm^{-1}$), once *Sr* is directly proportional to ΔE, Equation (9). In this work, it has been not observed expressive emission coming from $^5D_1$ excited level. Therefore, $^7F_2$ and $^7F_0$ thermally coupled energy levels were used, which provided a remarkable performance, similar to other thermometers based on the same approach (Table 1).

$$S_r = \frac{1}{LIR}\left|\frac{\partial LIR}{\partial T}\right| = \frac{\Delta E}{k_B T^2} \times 100 \tag{9}$$

The error of the relative thermal sensitivity was obtained using Equation (10) [38].

$$\delta Sr = Sr\sqrt{\left(\frac{\delta \Delta E}{\Delta E}\right)^2 + \left(-2\frac{\delta T}{T}\right)^2} \tag{10}$$

Temperature uncertainty (δT) of the thermometer is the temperature resolution, *i.e*, the smallest temperature change that can be detected in each measurement [26,38]. The temperature uncertainty is given by Equation (11).

$$\delta T = \frac{1}{S_r}\frac{\delta LIR}{LIR} \tag{11}$$

where δLIR/LIR is the relative error in the thermometric parameter. Temperature uncertainty of 1.7 K was obtained at 300 K.

To attest the long-term thermal stability, BGeB-30%wst glass sample was submitted to cyclic temperature changes, in accordance with established methodologies for luminescence thermometers [38,49,50]. Figure SI5 presents the PL emission spectra after excitation at 393.5 nm (a) and 610.0 nm (a), at 300 K and 400 K. Although a slight fluctuation in the absolute intensity occurs for the same temperature throughout the cycles, it happens for both 393.5 nm and 610.0 nm excitations. Thus, the ratiometric thermometry circumvent these fluctuations and no significant LIR change will be observed. Indeed, as can be seen in Fig. 6c, BGeB-30%wst glass sample proved to be stable under twelve consecutive heating-cooling cycles, with a mean LIR value of 0.16545 and a standard deviation of only 0.00277 (RSD = 1.67%) at 400 K. The bottom and top edges of the cyan rectangle in Fig. 6c are the mean values for LIR at 300 K and 400 K, respectively.

4. Conclusions

Recovering rare-earth elements from electronic waste offers a sustainable source for such functional materials. In this work, it has been demonstrated that borogermanate glass doped with europium ion recovered from electronic waste constitute a practicable and sustainable platform for luminescence thermometry applications. Borogermanate glasses doped with Eu^{3+} ions were prepared via melt-quenching and characterized. The photoluminescent behavior for temperature sensing was explored. The glass exhibited characteristic Eu^{3+} emission transitions with temperature-dependent luminescence intensity ratio (LIR) between thermally coupled $^7F_0$ and $^7F_2$ energy levels, following Boltzmann distribution in the 300–400 K range. The energy gap was determined as $926 \pm 44\ cm^{-1}$, with a maximum relative thermal sensitivity of $1.48\ \%\ K^{-1}$ at 300 K and a temperature uncertainty of 1.7 K. In summary, the results proved that incorporating Eu^{3+} ion recovered from fluorescent lamps waste to borogermanate glass provides not only an environmentally suitable approach but also a high value-added functional material for optical sensing technologies.

CRediT authorship contribution statement

Fábio J. Caixeta: Conceptualization, Data curation, Formal analysis, Investigation, Methodology, Writing – original draft, Writing – review & editing. **Ana Elisa Berno:** Data curation, Formal analysis, Methodology, Writing – original draft. **Marina P. Abuçafy:** Conceptualization, Investigation, Methodology, Writing – original draft, Writing – review & editing. **Elias P. Ferreira-Neto:** Conceptualization, Funding acquisition, Project administration, Writing – original draft, Writing – review & editing. **Leonardo V. Albino:** Methodology, Writing – original draft, Writing – review & editing. **Thiago A. Lodi:** Formal analysis, Methodology, Writing – original draft, Writing – review & editing. **Marcelo Nalin:** Conceptualization, Funding acquisition, Project administration, Supervision, Writing – original draft, Writing – review & editing. **Estevam C. Marques:** Data curation, Methodology, Writing – original draft. **Aline M. Feltran:** Data curation, Methodology, Writing – original draft. **Ana Beatriz Acosta:** Data curation, Methodology, Writing – original draft. **Vitor dos S.de Souza:** Data curation, Methodology, Writing – original draft. **Rogéria R. Gonçalves:** Conceptualization, Funding acquisition, Supervision, Writing – original draft, Writing – review & editing. **Sidney J.L. Ribeiro:** Conceptualization, Formal analysis, Funding acquisition, Investigation, Methodology, Project administration, Resources, Supervision, Validation, Visualization, Writing – original draft, Writing – review & editing. **Douglas F. Franco:** Conceptualization, Formal analysis, Funding acquisition, Investigation,

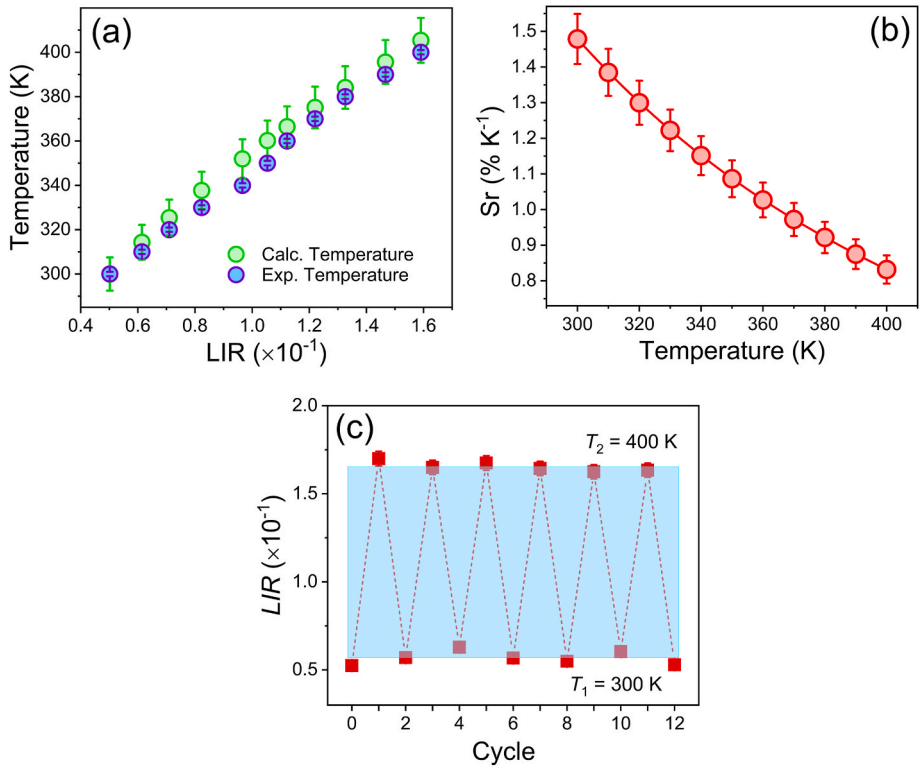

Fig. 6. (a) Calculated and experimental temperatures versus *LIR*. (b) Relative thermal sensitivity versus experimental temperature. (c) Cycling the luminescent intensity ratio in the 300-400 K range.

Table 1
Relative thermal sensitivity (Sr, % K^{-1}) for various luminescence thermometers based on Eu^{3+} thermally coupled energy levels.

Material	Therm. Coupled levels	ΔE (cm^{-1})	Max. Sr (% K^{-1})	Ref.
BGeB:Eu^{3+}	$^7F_0$, $^7F_2$	926 and 1002	1.48 at 300 K	This work
$(NaPO_3)_3$-$Al(PO_3)_3$:Eu^{3+}	$^7F_0$, $^7F_2$	969 and 1036	1.68 at 288 K	[42]
Y_2O_3:Eu^{3+}	$^7F_1$, $^7F_2$	875	1.7 at 323 K	[25]
TeO_2-Li_2CO_3/H_3BO_3-Li_2CO_3-$CaCO_3$:Eu^{3+}	$^5D_1$, $^5D_0$	1762	2.75 at 293 K	[45]
$CaWO_4$:Eu^{3+}	$^5D_1$, $^5D_0$	1538	0.9 at 425 K	[28]
$Y_2Mo_3O_{12}$:Eu^{3+}	$^5D_1$, $^5D_0$	———	0.5 at 472 K	[46]
$CaSr_2(PO_4)_2$:Eu^{3+}	$^5D_1$, $^5D_0$	1610	2.227 at 323 K	[47]
$Gd_2Ti_2O_7$:Eu^{3+}	$^5D_1$, $^5D_0$	1718	0.95 at 423 K	[48]

Methodology, Project administration, Supervision, Validation, Writing – original draft, Writing – review & editing.

Declaration of competing interest

The authors declare that they have no known competing financial interests or personal relationships that could have appeared to influence the work reported in this paper.

Acknowledgments

The authors acknowledge São Paulo Research Foundation (FAPESP, grant numbers 2013/07793-6, 2023/04832-2, 2024/13104-3, 2025/08960-0, 2025/05131-3) and National Council for Scientific and Technological Development (CNPq, grant number 407747/2022-2). F. J. Caixeta acknowledges CNPq (grant numbers 380556/2023-5 and 385050/2023-2). L. V. Albino personally acknowledges funding by FAPESP (grant number 2025/14080-3), CNPq, and National System of Photonics Laboratories (Sisfóton, grant 384430/2024-4). INCT-INFO (National Institute of Photonics) and INCT NanoVida (Nanomaterials for Life) are also acknowledged. Authors acknowledge Prof. Marco Aurélio Cebim and Luminescent Materials Laboratory, Institute of Chemistry, São Paulo State University (UNESP) for the thermometric measurements' facilities.

Appendix A. Supplementary data

Supplementary data to this article can be found online at https://doi.org/10.1016/j.jlumin.2026.121831.

Data availability

Data will be made available on request.

References

[1] S. Meredith, The global critical minerals race is heating up — and rare earths stocks are skyrocketing, CNBC 1 (2025). https://www.cnbc.com/2025/11/03/rare-earths-stocks-boom-as-the-global-critical-mineral-race-heats-up.html. (Accessed 4 November 2025).
[2] P. Wang, Y.-Y. Yang, O. Heidrich, L.-Y. Chen, L.-H. Chen, T. Fishman, W.-Q. Chen, Regional rare-earth element supply and demand balanced with circular economy strategies, Nat. Geosci. 17 (2024) 94–102, https://doi.org/10.1038/s41561-023-01350-9.
[3] J.-C.G. Bünzli, K.-L. Wong, Lanthanide photonics on the path to future: from gas lighting to optical computers, J. Lumin. 287 (2025) 121473, https://doi.org/10.1016/j.jlumin.2025.121473.
[4] W.A. de Oliveira, A.G. Bispo-Jr, B.F.D. Aquino, D.A. Hora, M.S.C. de Oliveira, A.J. S. Silva, N.S. Ferreira, F.A. Sigoli, M.V. dos S. Rezende, Upconversion emission and temperature sensing properties of the LiBaPO4: Er^{3+}, Yb^{3+} phosphor, Opt. Mater. 160 (2025) 116700, https://doi.org/10.1016/j.optmat.2025.116700.
[5] R.F. Salgueiro, F.E. Maturi, V.M.P. da Silva, D. Manzani, C.D.S. Brites, Ln^{3+}-doped glasses: advancing molecular logic for integration into photonic and electronic devices, J. Lumin. 277 (2025) 120932, https://doi.org/10.1016/j.jlumin.2024.120932.

[6] K. Huang, J. Fung-A-Fat, J. Wu, S. Yu, D. Fung-A-Fat, K. Deng, G. Zuercher, D. Sankar, I. Saroha, W. Xu, G. Han, Lanthanide-based quantum optical materials, Adv. Funct. Mater. n/a (2025) e24562, https://doi.org/10.1002/adfm.202524562.

[7] G. Tessitore, G.A. Mandl, S.L. Maurizio, M. Kaur, J.A. Capobianco, The role of lanthanide luminescence in advancing technology, RSC Adv. 13 (2023) 17787–17811, https://doi.org/10.1039/D3RA00991B.

[8] A.K. Hamzat, M.S. Murad, B. Subeshan, R. Asmatulu, E. Asmatulu, Rare earth element recycling: a review on sustainable solutions and impacts on semiconductor and chip industries, J. Mater. Cycles Waste Manag. 27 (2025) 3009–3032, https://doi.org/10.1007/s10163-025-02276-7.

[9] D. Woods, A stackelberg model of china's rare earths strategic lead, J. Chinese polit, Science (2025), https://doi.org/10.1007/s11366-025-09921-w.

[10] S. Gulliani, M. Volpe, A. Messineo, R. Volpe, Recovery of metals and valuable chemicals from waste electric and electronic materials: a critical review of existing technologies, RSC Sustain. 1 (2023) 1085–1108, https://doi.org/10.1039/D3SU00034F.

[11] Y.-H. Han, X.-W. Cui, Y. Zhang, H. Zhang, Z. Chen, Environmental impacts of rare earth elements mining and strategies for sustainable management: a comprehensive review, J. Hazard. Mater. 500 (2025) 140400, https://doi.org/10.1016/j.jhazmat.2025.140400.

[12] A.E. Berno, F.J. Caixeta, J.P.C. Ruzene, A.M. Feltran, L. V Albino, M.P. Abuçafy, O. de B. Silva, J.P.P. Rodrigues, E.P. Ferreira-Neto, A.P.A. Rosa, D. Bevilaqua, M. Nalin, S.J.L. Ribeiro, D.F. Franco, Recycled rare Earth ions from E-Waste in borogermanate glasses for magneto-optical applications, Chem. Asian J. 20 (2025) e202401613, https://doi.org/10.1002/asia.202401613.

[13] L.H. Xavier, M. Ottoni, L.P.P. Abreu, A comprehensive review of urban mining and the value recovery from e-waste materials, Resour. Conserv. Recycl. 190 (2023) 106840, https://doi.org/10.1016/j.resconrec.2022.106840.

[14] D.F. Franco, F.J. Caixeta, L. V Albino, T.A. Lodi, J.R. Orives, E.O. Ghezzi, M. Nalin, Optical materials : x terbium-doped transparent glass-ceramics containing $TbPO_4$ crystals : a promising material for photonic applications, Opt. Mater. X 20 (2023) 100272, https://doi.org/10.1016/j.omx.2023.100272.

[15] Y. Guo, J. Canning, Z. Chaczko, G.-D. Peng, A magneto-optical fibre transducer, Proc. SPIE (2025) 136399E, https://doi.org/10.1117/12.3061813.

[16] D.F. Franco, R.G. Fernandes, J.F. Felix, V.R. Mastelaro, H. Eckert, C.R.M. Afonso, Y. Messaddeq, S.H. Messaddeq, S. Morency, M. Nalin, Fundamental studies of magneto-optical borogermanate glasses and derived optical fibers containing Tb^{3+}, J. Mater. Res. Technol. 11 (2021) 312–327, https://doi.org/10.1016/j.jmrt.2021.01.010.

[17] C.D.S. Brites, P.P. Lima, N.J.O. Silva, A. Millán, V.S. Amaral, F. Palacio, L.D. Carlos, Thermometry at the nanoscale, Nanoscale 4 (2012) 4799–4829, https://doi.org/10.1039/C2NR30663H.

[18] D. Jaque, F. Vetrone, Luminescence nanothermometry, Nanoscale 4 (2012) 4301–4326, https://doi.org/10.1039/C2NR30764B.

[19] C.D.S. Brites, S. Balabhadra, L.D. Carlos, Lanthanide-based thermometers: at the cutting-edge of luminescence thermometry, Adv. Opt. Mater. 7 (2019) 1801239, https://doi.org/10.1002/adom.201801239.

[20] R. Usamentiaga, P. Venegas, J. Guerediaga, L. Vega, J. Molleda, F.G. Bulnes, Infrared thermography for temperature measurement and non-destructive testing, Sensors 14 (2014) 12305–12348, https://doi.org/10.3390/s140712305.

[21] M. Vollmer, K.P. Möllmann, Infrared Thermal Imaging, John Wiley & Sons, 2018. https://api.semanticscholar.org/CorpusID:140058451.

[22] A. Nexha, J.J. Carvajal, M.C. Pujol, F. Díaz, M. Aguiló, Lanthanide doped luminescence nanothermometers in the biological windows: strategies and applications, Nanoscale 13 (2021) 7913–7987, https://doi.org/10.1039/D0NR09150B.

[23] S.A. Wade, S.F. Collins, G.W. Baxter, Fluorescence intensity ratio technique for optical fiber point temperature sensing, J. Appl. Phys. 94 (2003) 4743–4756, https://doi.org/10.1063/1.1606526.

[24] L. Carlos, R. Ferreira, V. Bermudez, S. Ribeiro, Lanthanide-containing light-emitting organic-inorganic hybrids: a bet on the future, Adv. Mater. 21 (2009) 509–534, https://doi.org/10.1002/adma.200801635.

[25] A.S. Souza, L.A.O. Nunes, I.G.N. Silva, F.A.M. Oliveira, L.L. da Luz, H.F. Brito, M.C. F.C. Felinto, R.A.S. Ferreira, S.A. Júnior, L.D. Carlos, O.L. Malta, Highly-sensitive Eu^{3+} ratiometric thermometers based on excited state absorption with predictable calibration, Nanoscale 8 (2016) 5327–5333, https://doi.org/10.1039/C6NR00158K.

[26] F.J. Caixeta, A.R.N. Bastos, A.M.P. Botas, L.S. Rosa, V.S. Souza, F.H. Borges, A.N. C. Neto, A. Ferrier, P. Goldner, L.D. Carlos, R.R. Gonçalves, R.A.S. Ferreira, High-quantum-yield upconverting Er^{3+}/Yb^{3+} -Organic–Inorganic hybrid dual coatings for real-time temperature sensing and photothermal conversion, J. Phys. Chem. C 124 (2020) 19892–19903, https://doi.org/10.1021/acs.jpcc.0c03874.

[27] F.H. Borges, J.C. Martins, F.J. Caixeta, L.D. Carlos, R.A.S. Ferreira, R.R. Gonçalves, Luminescent thermometry based on Er^{3+}/Yb^{3+} co-doped yttrium niobate with high NIR emission and NIR-to-visible upconversion quantum yields, J. Lumin. 248 (2022) 118986, https://doi.org/10.1016/j.jlumin.2022.118986.

[28] L. Li, Y. Zhou, F. Qin, J. Miao, Y. Zheng, Z. Zhang, Eu^{3+}-based luminescence ratiometric thermometry, RSC Adv. 10 (2020) 9444–9449, https://doi.org/10.1039/D0RA00170H.

[29] X. Wang, Q. Liu, Y. Bu, C.-S. Liu, T. Liu, X. Yan, Optical temperature sensing of rare-earth ion doped phosphors, RSC Adv. 5 (2015) 86219–86236, https://doi.org/10.1039/C5RA16986K.

[30] S.O. Adeleye, A.A. Adeleke, P. Nzerem, A.I. Olosho, E.N. Anosike-Francis, T. S. Ogedengbe, P.P. Ikubanni, R.A. Saleh, J.A. Okolie, A review of the physical, optical and photoluminescence properties of rare Earth ions doped glasses, Trends Sci. 21 (2024) 8759, https://doi.org/10.48048/tis.2024.8759.

[31] K.S. Serkina, D. V Volkova, K.I. Runina, I. V Stepanova, Synthesis and spectral-luminescent properties of sodium-modified bismuth germanate glasses, Glas. Ceram. 81 (2024) 267–271, https://doi.org/10.1007/s10717-024-00694-x.

[32] D.F. Franco, S. Morency, Y. Messaddeq, M. Nalin, Multimode magneto-optical fiber based on borogermanate glass containing Tb^{3+} for sensing applications, Materials 18 (2025) 4736, https://doi.org/10.3390/ma18204736.

[33] F.R. Henrique, A.G. Pelosi, J.M.P. Almeida, D.F. Franco, L.H.Z. Cocca, J.L. Clabel, M. Nalin, V.R. Mastelaro, L. De Boni, C.R. Mendonça, Nonlinear refraction in high terbium content borogermanate glass bulk and fiber, Opt. Mater. 147 (2024) 114635, https://doi.org/10.1016/j.optmat.2023.114635.

[34] P.R. Babu, D. Gelija, K.S. Pasupuleti, B.K. Kumar, N.J. Sushma, M.-D. Kim, B.D. P. Raju, Optical, emission, and excitation dynamics of Eu^{3+}-doped bismuth-based phosphate glass for visible display laser applications, Luminescence 38 (2023) 71–82, https://doi.org/10.1002/bio.4422.

[35] J. Mooney, P. Kambhampati, Get the basics right: jacobian conversion of wavelength and energy scales for quantitative analysis of emission spectra, J. Phys. Chem. Lett. 4 (2013) 3316–3318, https://doi.org/10.1021/jz401508t.

[36] K. Binnemans, Interpretation of europium(III) spectra, Coord. Chem. Rev. 295 (2015) 1–45, https://doi.org/10.1016/j.ccr.2015.02.015.

[37] W.T. Carnall, G.L. Goodman, K. Rajnak, R.S. Rana, A systematic analysis of the spectra of the lanthanides doped into single crystal LaF3, J. Chem. Phys. 90 (1989) 3443–3457, https://doi.org/10.1063/1.455853.

[38] C.D.S. Brites, A. Millán, L.D. Carlos, Handbook on the physics and chemistry of rare earths, Elsevier 49 (2016) 339–427, https://doi.org/10.1016/bs.hpcre.2016.03.005.

[39] R.G. Geitenbeek, H.W. de Wijn, A. Meijerink, Non-boltzmann luminescence in $NaYF_4$:Eu^{3+}: implications for luminescence thermometry, Phys. Rev. Appl. 10 (2018) 64006, https://doi.org/10.1103/PhysRevApplied.10.064006.

[40] P. Atkins, J. de Paula, Physical Chemistry, eighth ed., Oxford University Press, New York, 2006.

[41] D.A. McQuarrie, Statistical Mechanics, first ed., University Science Books, Melville, 2000.

[42] C.Y. Morassuti, L.A.O. Nunes, S.M. Lima, L.H.C. Andrade, Eu^{3+}- doped alumino-phosphate glass for ratiometric thermometer based on the excited state absorption, J. Lumin. 193 (2018) 39–43, https://doi.org/10.1016/j.jlumin.2017.09.001.

[43] A. Savitzky, M.J.E. Golay, Smoothing and differentiation of data by simplified least squares procedures, Anal. Chem. 36 (1964) 1627–1639, https://doi.org/10.1021/ac60214a047.

[44] K. Binnemans, C. Görller-Walrand, Application of the Eu^{3+} ion for site symmetry determination, J. Rare Earths 14 (1996) 173–180.

[45] V.K. Rai, A. Rai, Temperature sensing behavior of Eu^{3+} doped tellurite and calibo glasses, Appl. Phys. B 86 (2007) 333–335, https://doi.org/10.1007/s00340-006-2445-1.

[46] T. Gavrilović, V. Đorđević, J. Periša, M. Medić, Z. Ristić, A. Ćirić, Ž. Antić, M. D. Dramićanin, Luminescence thermometry with Eu^{3+}-Doped $Y_2Mo_3O_{12}$: comparison of performance of intensity ratio and machine learning temperature read-outs, Materials 17 (2024) 5354, https://doi.org/10.3390/ma17215354.

[47] R. Singh, M. Manhas, A.K. Bedyal, F. Durani, H.C. Swart, V. Kumar, Thermometric and luminescence studies of Eu^{3+} activated $CaSr_2(PO_4)_2$ phosphor for non-contact optical thermometry and solid state lighting applications, Mater. Chem. Phys. 291 (2022) 126735, https://doi.org/10.1016/j.matchemphys.2022.126735.

[48] V. Lojpur, S. Ćulubrk, M.D. Dramićanin, Ratiometric luminescence thermometry with different combinations of emissions from Eu^{3+} doped $Gd_2Ti_2O_7$ nanoparticles, J. Lumin. 169 (2016) 534–538, https://doi.org/10.1016/j.jlumin.2015.01.027.

[49] S. Balabhadra, M.L. Debasu, C.D.S. Brites, R.A.S. Ferreira, D. Carlos, Upconverting Nanoparticles Working As Primary Thermometers In Di ff erent Media. https://doi.org/10.1021/acs.jpcc.7b04827, 2017.

[50] S. Laia, F.J.R. Tavares, M.S.C. De Oliveira, V. Marcos, S. Rezende, I. De Fatima, J. Rodrigues, A.R.C. Alencar, Luminescent thermometry with YVO 4 : er/Nd : achieving high sensitivities within the 1st and 2nd biological windows, 265, https://doi.org/10.1016/j.jlumin.2023.120239, 2024.